

LETTER TO THE EDITOR

Resolving the cold debris disc around a planet-hosting star[★] PACS photometric imaging observations of q¹ Eridani (HD 10647, HR 506)

R. Liseau¹, C. Eiroa², D. Fedele^{2,3,4}, J.-C. Augereau⁵, G. Olofsson⁶, B. González⁷, J. Maldonado², B. Montesinos⁸, A. Mora^{2,9}, O. Absil¹⁰, D. Ardila¹¹, D. Barrado^{8,12}, A. Bayo^{8,24}, C. A. Beichman¹³, G. Bryden¹⁴, W. C. Danchi¹⁵, C. del Burgo¹⁶, S. Ertel¹⁷, C. W. M. Fridlund¹⁸, A. M. Heras¹⁸, A. V. Krivov¹⁹, R. Launhardt³, J. Lebreton⁵, T. Löhne¹⁹, J. P. Marshall²⁰, G. Meeus², S. Müller¹⁹, G. L. Pilbratt¹⁸, A. Roberge¹⁵, J. Rodmann²¹, E. Solano⁸, K. R. Stapelfeldt¹⁴, Ph. Thébault²², G. J. White^{20,23}, and S. Wolf¹⁷

(Affiliations are available in the online edition)

Received 31 March 2010 / Accepted 16 April 2010

ABSTRACT

Context. About two dozen exo-solar debris systems have been spatially resolved. These debris discs commonly display a variety of structural features such as clumps, rings, belts, eccentric distributions and spiral patterns. In most cases, these features are believed to be formed, shaped and maintained by the dynamical influence of planets orbiting the host stars. In very few cases has the presence of the dynamically important planet(s) been inferred from direct observation.

Aims. The solar-type star q¹ Eri is known to be surrounded by debris, extended on scales of $\lesssim 30''$. The star is also known to host at least one planet, albeit on an orbit far too small to make it responsible for structures at distances of tens to hundreds of AU. The aim of the present investigation is twofold: to determine the optical and material properties of the debris and to infer the spatial distribution of the dust, which may hint at the presence of additional planets.

Methods. The Photodetector Array Camera and Spectrometer (PACS) aboard the *Herschel* Space Observatory allows imaging observations in the far infrared at unprecedented resolution, i.e. at better than $6''$ to $12''$ over the wavelength range of $60\ \mu\text{m}$ to $210\ \mu\text{m}$. Together with the results from ground-based observations, these spatially resolved data can be modelled to determine the nature of the debris and its evolution more reliably than what would be possible from unresolved data alone.

Results. For the first time has the q¹ Eri disc been resolved at far infrared wavelengths. The PACS observations at $70\ \mu\text{m}$, $100\ \mu\text{m}$ and $160\ \mu\text{m}$ reveal an oval image showing a disc-like structure in all bands, the size of which increases with wavelength. Assuming a circular shape yields the inclination of its equatorial plane with respect to that of the sky, $i > 53^\circ$. The results of image de-convolution indicate that i likely is larger than 63° , where 90° corresponds to an edge-on disc.

Conclusions. The observed emission is thermal and optically thin. The resolved data are consistent with debris at temperatures below 30 K at radii larger than 120 AU. From image de-convolution, we find that q¹ Eri is surrounded by an about 40 AU wide ring at the radial distance of ~ 85 AU. This is the first real Edgeworth-Kuiper Belt analogue ever observed.

Key words. stars: individual: q¹ Eri (HD 10647, HR 506, HIP 7978) – planetary systems – stars: formation – circumstellar matter

1. Introduction

We report new observations of the debris disc around q¹ Eri (HD 10647, HR 506) using the *Herschel* Space Observatory (Pilbratt et al. 2010). The observations form part of a larger key programme (KP), viz. DUNES¹, which is described in more detail by Eiroa et al. (2010). Here, we give a brief summary to put the contents of this Letter into context. The DUNES KP is a sensitivity limited study with the goal of discovering and characterising extra-solar analogues of the Edgeworth-Kuiper belt (EKB) in an unbiased, statistical sample of nearby F, G and K main-sequence stars. The sample is volume limited, with distances $\lesssim 20$ pc, and spans a broad range of stellar ages, from ~ 0.1

to roughly 10 Gyr. In addition to the object of the present study (q¹ Eri), a number of M- and A-type stars will be observed in collaboration with the DEBRIS-KP team (Matthews et al. 2010), implying that the whole sample covers a decade in stellar mass from 0.2 to $2 M_\odot$.

The PACS (Poglitsch et al. 2010) observations at $100\ \mu\text{m}$ aim at the detection of the stellar photospheres down to the confusion noise with a signal to noise ratio (S/N) of at least 5. Together with observations in the other *Herschel* bands, this will lead to an unprecedented characterisation of discs and will allow detailed theoretical modelling. It is foreseen that fractional luminosities L_{dust}/L_\odot of a few times 10^{-7} will be reached, i.e. similar to that of the EKB of the Solar System (Stern 1996; Jewitt et al. 2009) and a more than order of magnitude improvement over *Spitzer* data (Bryden et al. 2009).

A main-sequence star with an infrared excess larger by more than three orders of magnitude than this limit is the late F-type star q¹ Eri. This will potentially allow to study the material

[★] *Herschel* is an ESA space observatory with science instruments provided by European-led Principal Investigator consortia and with important participation from NASA.

¹ DUst around NEarby Stars,
<http://www.mpia-hd.mpg.de/DUNES/>.

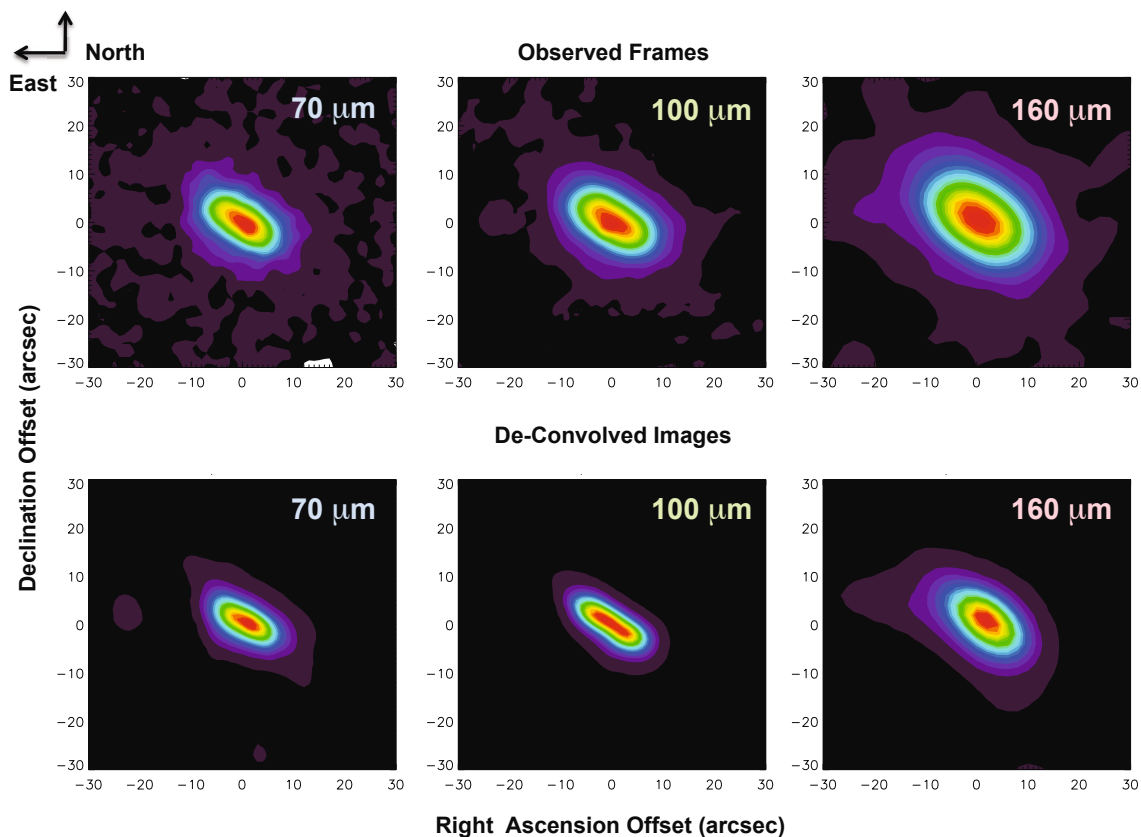


Fig. 1. PACS photometric imaging of q^1 Eri at, from left to right, $70\ \mu\text{m}$ (blue), $100\ \mu\text{m}$ (green) and $160\ \mu\text{m}$ (red). The $70\ \mu\text{m}$ image was taken in chop-nod mode, whereas the other two in scan-map mode. The upper panels display the reduced observations. Below, de-convolved images are shown, using observations of α Boo for the definition of the PSF. Displayed are the results for ten iterations of a MEM algorithm (Hollis et al. 1992). The star defines the origin of the frames, i.e. offset coordinates (0,0). Within the positional accuracy ($2''$ rms), the stellar position and the centre of the elliptical brightness distributions coincide (see Table 1) and offsets are in seconds of arc. The lowest contours are at 5% of the maximum values and consecutive steps are also by this amount. At the distance of the star, $20''$ corresponds to 350 AU.

giving rise to the excess in great detail. The star is known to be accompanied by a giant planet, q^1 Eri b, orbiting at the distance of 2 AU (Butler et al. 2006, and references therein), which corresponds to $0''.1$ at the distance of the system (17.35 pc; Perryman et al. 1997; van Leeuwen 2007). Such a small angle will not be resolved by the observations described in this paper, but q^1 Eri is also surrounded by a ring or belt system of scattering and thermally emitting dust particles. The extent of the system, which from optical to sub-millimetre wavelengths is up to several tens of arc seconds in size (e.g., Stapelfeldt et al. 2007; Liseau et al. 2008, and references therein), should be readily accessible to PACS at the *Herschel* telescope ($\theta''_{\text{diff}} = 7 \times \lambda_{\mu\text{m}}/100\ \mu\text{m}$).

This contribution presents the observed properties of the q^1 Eri system by *Herschel*. The results of theoretical model calculations will be communicated by Augereau et al. (in prep.). The observations and data reduction are described in Sect. 2, with the results presented in Sect. 3. These are discussed in Sect. 4 and, finally in Sect. 5, our main conclusions are briefly summarised.

2. Observations and data reduction

During this initial observing run, two different modes of observing were executed for test reasons, in order to optimise the efficiency of the programme in terms of observing time and signal-to-noise ratio (S/N). These modes were, respectively, the chop-and-nod mode (70 , 100 and $160\ \mu\text{m}$), adopted for point source observing, and the scan-map option (100 and $160\ \mu\text{m}$), for

extended sources (Fig. 1). These modes are described by Eiroa et al. (2010) and in a future technical note.

The reduction was done within the *Herschel* interactive processing environment, using HIPE_v2.0.0_RC3, and with scripts for the pipeline developed by members of the PACS-ICC². At the medium scan speed of $20''\ \text{s}^{-1}$, two maps along position angles 63° and 117° , respectively, were obtained in order to minimise striping in the resultant images. At both $100\ \mu\text{m}$ and $160\ \mu\text{m}$, the sky noise was lower in the scan-map data (2.8 and 5.2) $\times 10^{-5}\ \text{Jy arcsec}^{-2}$, respectively, as compared to (3.9 and 12) $\times 10^{-5}\ \text{Jy arcsec}^{-2}$ of the chop-nod observations. These values are comparable to the surface brightness of the scattering disc at $0.6\ \mu\text{m}$ ($1.3 \times 10^{-5}\ \text{Jy arcsec}^{-2}$, as deduced from data in Stapelfeldt et al. 2007).

The prime calibrator Arcturus (α Boo; e.g., Cohen et al. 2005) was observed close in time with q^1 Eri and was used to provide the instrumental point spread function (PSF)³.

The filters at the reference wavelengths of 70 , 100 and $160\ \mu\text{m}$ are referred to as *blue*, *green* and *red*, spanning 60 – $85\ \mu\text{m}$, 85 – $130\ \mu\text{m}$ and 130 – $210\ \mu\text{m}$, respectively

² *Herschel* science demonstration phase data processing workshop, 14–16 December 2009, ESAC, Spain.

³ See <http://Herschel.esac.esa.int/AOTsReleaseStatus.shtml>

http://Herschel.esac.esa.int/Docs/AOTsReleaseStatus/PACS_ScanChopNod_ReleaseNote_22Feb2010.pdf

http://Herschel.esac.esa.int/Docs/AOTsReleaseStatus/PACS_PhotMap_ReleaseNote_23Feb2010.pdf

Table 1. Brightness, orientation and extent of the q^1 Eri debris system.

Observation ID and Mode	$\Delta RA, \Delta Dec^a$ (" , ")	Flux ^b (mJy)	$2a^b$ (")	$2b^b$ (")	PA ^c (°)	i^d (°)	Alternate flux measurement (mJy)
1342187142 – 70 : chop-nod	+0.9, –0.9	828 ± 83	13.9 (11.0)	7.9 (4.4)	54.4 (60.0)	55.4 (66.4)	859 ± 6 <i>Spitzer</i> /MIPS ^e
1342187141 – 100: chop-nod	+2, 0	816 ± 82	15.5 (12.6)	8.8 (5.1)	54.4 (56.2)	55.4 (66.1)	1080 ± 36 IRAS FSC
134218739/40 – 100: scan map	0, –1.4	810 ± 81	15.1 (12.5)	8.8 (4.7)	56.1 (54.8)	54.4 (67.9)	1080 ± 36 IRAS FSC
1342187142 – 160: chop-nod	–1.4, +0.9	529 ± 106	18.9 (13.5)	12.3 (7.8)	51.3 (48.9)	49.4 (54.7)	453 ± 50 <i>Spitzer</i> /MIPS ^f
134218739/40 – 160: scan map	+1.4, –1.6	537 ± 107	19.3 (13.3)	12.5 (6.5)	51.2 (55.7)	49.6 (60.7)	453 ± 50 <i>Spitzer</i> /MIPS ^f

Notes. ^(a) Offsets of ellipse centre relative to stellar coordinates: proper motion corrected to IRCS 2009.89 (+0.186 s and $-1'055$ [Perryman et al. 1997](#); [van Leeuwen 2007](#)) $01^h42^m29^s.502$, $-53^\circ 44' 28''.06$. The photospheric fluxes are 17 mJy at $70 \mu\text{m}$, 8 mJy at $100 \mu\text{m}$ and 3 mJy at $160 \mu\text{m}$ (cf. Fig. 2).

^(b) Flux for Gaussian ellipse with fitted FWHM to major and minor axis, $2a$ and $2b$, respectively. Values in parentheses refer to de-convolved images.

^(c) Position angle measured from North over East.

^(d) Lower limit to the inclination, where $i = 90^\circ$ refers to an edge-on geometry.

^(e) [Trilling et al. \(2008\)](#).

^(f) [Tanner et al. \(2009\)](#).

([Poglitsch et al. 2008](#)). The PSF has a tripolar shape at low intensities, i.e. a few percent of the peak value, and the half-power-width is circular for the $70 \mu\text{m}$ and $100 \mu\text{m}$ filters, but somewhat elongated at $160 \mu\text{m}$ in the scan direction. Currently, the estimated accuracy of the absolute flux calibration is estimated to be better than 20% in the long-wave and better than 10% in the short-wave bands.

3. Results

In the Scan Map AOT release is the following note: *The fluxes are too high and have to be scaled down by the following factors 1.05 in the blue band, 1.09 in the green band 1.29 in the red band, and in Table 1, no colour correction has been applied to the reported fluxes. The internal consistency of the PACS data – at a given wavelength but for different observing modes – is strikingly good and lends confidence to the quality of these data. From the comparison with previous measurements, it is apparent that IRAS fluxes are on the high side, whereas long-wave *Spitzer* data are somewhat on the low side.*

At the level of the pointing accuracy of *Herschel* ($2''$ rms, corresponding to 35 AU), there is no significant offset of the centres of the elliptical isophotes with respect to the position of the star (Table 1). This uncertainty is much larger than the offset of 8 AU observed for Fomalhaut ([Kalas et al. 2008](#)). For the nominal wavelengths of $70 \mu\text{m}$, $100 \mu\text{m}$ and $160 \mu\text{m}$, the angular resolution is limited to about $6''$, $7''$ and $11''.5$, respectively. The image of q^1 Eri seems clearly resolved, therefore, only in the long dimension.

The average of the position angle of the elliptical source is $PA = 54^\circ$ and the average of the lower limit to the inclination of an intrinsically circular feature (ring or belt) is $i > 53^\circ$, with estimated uncertainties of $\sim \pm 5^\circ$ ($i = 90^\circ$ for an edge-on geometry). For the de-convolved images (see below), the disc would be seen more edge-on and in this case, $i > 63^\circ$. This is consistent with the tilt derived from optical images of the light scattered off the disc ($i = 76^\circ$, [Stapelfeldt et al. 2007](#)).

4. Discussion

4.1. The spectral energy distribution (SED) revisited

Figure 2 is taken from the paper by [Liseau et al. \(2008\)](#), but with the PACS data included. The $70 \mu\text{m}$ and $100 \mu\text{m}$ fluxes fall essentially on top of the 60 K blackbody curve, shown as a solid line.

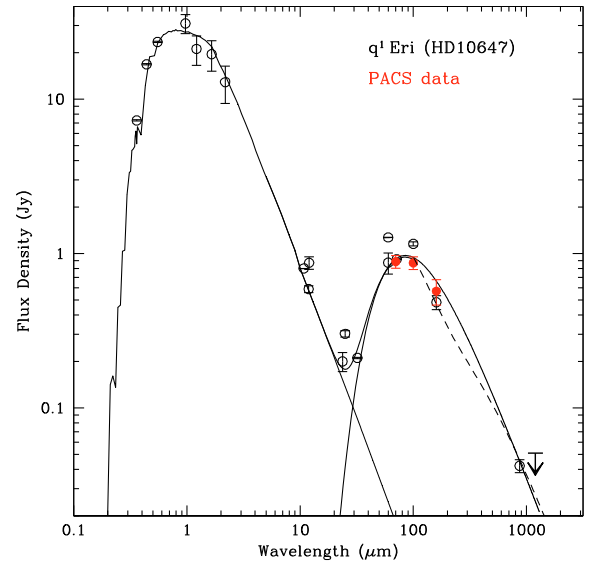


Fig. 2. This figure is similar to the SED of q^1 Eri shown in [Liseau et al. \(2008\)](#) with the difference that the PACS data of Table 1 are shown by the filled symbols. In addition, the $160 \mu\text{m}$ flux of *Spitzer* ([Tanner et al. 2009](#)) has also been added. As before, the solid curve for the IR excess is that of a single temperature blackbody ($\beta = 0$, where $\kappa_r \propto \nu^\beta$), and the dashed line refers to the ring-belt composite model of that paper.

For $160 \mu\text{m}$, the *Spitzer* observations of [Tanner et al. \(2009\)](#) are also included. These seemed to confirm the ring-belt model in our earlier paper. The new PACS datum is marginally below the blackbody, but also marginally above the composite SED and, at the moment, we need to leave this issue as undecided.

4.2. Image de-convolution

From high- S/N data, possible fine-structural details in the image can be retrieved. This would require image sharpening techniques, such as, e.g., image de-convolution with the known PSF.

The images were de-convolved with the rotated Arcturus-PSF using the algorithm for a maximum entropy method (MEM) developed by [Hollis et al. \(1992\)](#). Guided by experience, we stopped the routine after about a dozen iterations in order not to produce artefacts and/or false super-resolution. More automatic and/or quantitative methods were tried, but were eventually abandoned due to insufficient reliability. In Fig. 1, the direct

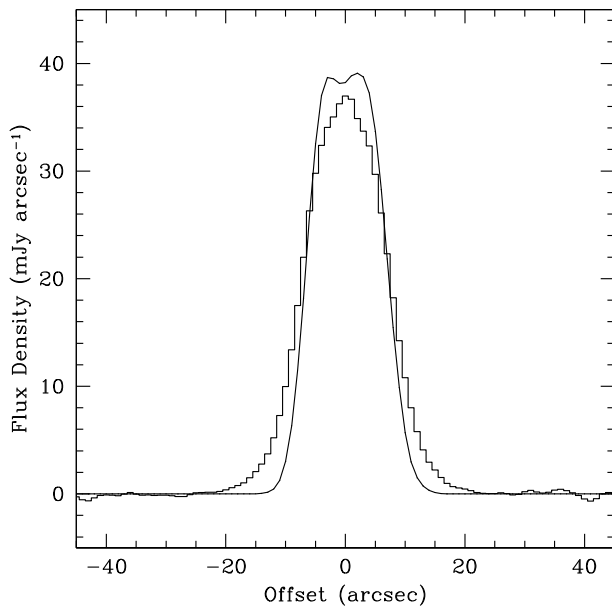


Fig. 3. One-dimensional cuts (averages of 5 pxl wide strips), along the major axis, through the $100\ \mu\text{m}$ scan map image, from which the stellar source has been subtracted prior to the de-convolution. The histogram depicts the observed data, whereas the smooth line shows the result of the applied de-convolution algorithm.

observations are compared with the de-convolved images and in Table 1, values measured on the sharpened images are reported.

In Fig. 3, one-dimensional cuts along the major axis of the observed and de-convolved $100\ \mu\text{m}$ image are displayed. It would have been more natural to select the observation at $70\ \mu\text{m}$, having the highest spatial resolution, but the $100\ \mu\text{m}$ scan map data are of considerably higher S/N , outweighing the apparent resolution advantage of the shorter wavelength data. In the analysed sub-frame, the flux was conserved within 7% by the MEM routine. Prior to the de-convolution, a stellar point source with photospheric flux of $8\ \text{mJy}$ at $100\ \mu\text{m}$ (Table 1) was subtracted from the PACS image. The resulting sharpened image reveals a central *broadened plateau* and a central depression with a depth of about 2%, which is consistent with the debris residing in a ring or belt around the star.

With standard assumptions regarding the emitting grains (astronomical silicates, a blow-out size limit $a_{\text{min}} = 0.6\ \mu\text{m}$ for the F9 V star and a -3.5 power law index for the size distribution) we find that the $100\ \mu\text{m}$ surface brightness profiles along the major and minor axes are well reproduced assuming a disk inclination of about 70° and a two-parameter model for the surface density, $\Sigma(r)$. These parameters are the peak density position, r_{max} , and the power law index of the surface density profile for $r > r_{\text{max}}$. The best fit to the surface brightness profiles is consistent with a ring-like disc, having values of $r_{\text{max}} \sim 85\ \text{AU}$ and $\Sigma(r > r_{\text{max}}) \propto r^{-3}$, respectively. A more elaborate model, with the size distribution computed self-consistently and taking into account the profiles also at other wavelengths, will be presented by Augereau et al. (in prep.).

This roughly $40\ \text{AU}$ wide ring or belt at about $85\ \text{AU}$ from the star appears similar to the EKB of the Solar System. Based on an analogy with the debris disc around Fomalhaut and on theoretical expectations, it is quite possible that another gas giant planet, $q^1\ \text{Eri}\ c$, could be orbiting the star inside the inner belt edge. Given the age of the system, $\approx 2\ \text{Gyr}$, the direct detection of $q^1\ \text{Eri}\ c$, for instance by means of coronagraphy, can be expected to be hard (see, e.g., Beichman et al. 2006).

5. Conclusions

Based on imaging observations with PACS in the three photometric bands at $70\ \mu\text{m}$, $100\ \mu\text{m}$ and $160\ \mu\text{m}$ we find that

- The debris around the solar-type star $q^1\ \text{Eri}$ has an oval-shaped brightness distribution, the size of which increases with the wavelength.
- The integrated flux density at these wavelengths leads to an SED which is in good agreement with earlier results.
- The very high signal-to-noise of the $100\ \mu\text{m}$ scan map is adequate to sharpen the image using an image de-convolution technique, revealing a ring-like structure with maximum surface density at $\sim 85\ \text{AU}$ from the star.
- With a width of about 35 to $45\ \text{AU}$, this ring or belt around the F9 V star $q^1\ \text{Eri}$ is similar to the Edgeworth-Kuiper belt around the Sun. This may hint at the presence of another planet, $q^1\ \text{Eri}\ c$.

Acknowledgements. We wish to acknowledge the support by the SNSB, the CNES, the PNP and the MICINN. In addition, we have benefited from HCSS / HSpot / HIPE which are joint developments by the *Herschel* Science Ground Segment Consortium, consisting of ESA, the NASA *Herschel* Science Center, and the HIFI, PACS and SPIRE consortia.

References

- Beichman, C. A., Bryden, G., Stapelfeldt, K. R., et al. 2006, *ApJ*, 652, 1674
 Bryden, G., Beichman, C. A., Carpenter, J. M., et al. 2009, *ApJ*, 705, 1226
 Butler, R. P., Wright, J. T., Marcy, G. W., et al. 2006, *ApJ*, 646, 505
 Cohen, M., Carbon, D. F., Welch, W. J., et al. 2005, *AJ*, 129, 2836
 Eiroa, C., et al. 2010, *A&A*, 518, L131
 Jewitt, D., Moro-Martín, A., & Lacerda, P. 2009, in *Astrophysics in the Next Decade*, ed. H. A. Thronson et al., *Ap&SS Proc.*, 63
 Hollis, J. M., Dorband, J. E., & Yusef-Zadeh, F. 1992, *ApJ*, 386, 293
 Kalas, P., Graham, J. R., Chiang, E., et al. 2008, *Science*, 322, 1345
 Liseau, R., Risacher, C., Brandeker, A., et al. 2008, *A&A*, 480, L47
 Matthews, B. C., et al. 2010, *A&A*, 518, L135
 Pilbratt, G. L., et al. 2010, *A&A*, 518, L1
 Perryman, M. A. C., Lindegren, L., Kovalevsky, J. et al., 1997, *A&A*, 323, L49
 Poglitsch, A., Waelkens, C., Bauer, O. H., et al. 2008, *SPIE*, 7010, 701005
 Poglitsch, A., et al. 2010, *A&A*, 518, L2
 Stapelfeldt, K., Krist, J., Bryden, G., & Chen C., 2007, in the *Spirit of Bernard Lyot: the Direct Detection of Planets and Circumstellar discs in the 21st Century*, ed. P. Kalas, University of California, Berkeley, CA, USA, 47
 Stapelfeldt, K. R., Bryden, G., Krist, J., et al. 2009, in *Exoplanets and discs: their Formation and Diversity*, ed. T. Usuda et al., *AIPC*, 1158, 43
 Stern, S. A. 1996, *AJ*, 112, 1203
 Tanner, A., Beichman, C., Bryden, G., Lisse, C., & Lawler, S. 2009, *ApJ*, 704, 109
 Trilling, D. E., Bryden, G., Beichman, C. A., et al. 2008, *ApJ*, 674, 1086
 van Leeuwen, F. 2007, *A&A*, 474, 653

-
- ¹ Onsala Space Observatory, Chalmers University of Technology, 439 92 Onsala, Sweden
e-mail: rene.liseau@chalmers.se
- ² Departamento de Física Teórica, C-XI, Facultad de Ciencias, Universidad Autónoma de Madrid, Cantoblanco, 28049 Madrid, Spain
- ³ Max Planck Institut für Astronomie, Königstuhl 17, 69117 Heidelberg, Germany
- ⁴ Johns Hopkins University Dept. of Physics and Astronomy, 3701 San Martin drive Baltimore, MD 21210 USA
- ⁵ Université Joseph Fourier/CNRS, Laboratoire d'Astrophysique de Grenoble, UMR 5571, Grenoble, France
- ⁶ Stockholm Observatory, AlbaNova University Center, Roslagstullsbacken 21, 106 91 Stockholm, Sweden
- ⁷ INSA at ESAC, 28691 Villanueva de la Cañada, Madrid, Spain
- ⁸ LAEX-CAB, Depto. Astrofísica, Centro de Astrobiología (INTA-CSIC), PO Box 78, 28691 Villanueva de la Cañada, Spain
- ⁹ ESA-ESAC Gaia SOC. PO Box 78, 28691 Villanueva de la Cañada, Madrid, Spain
- ¹⁰ Institut d'Astrophysique et de Géophysique, Université de Liège, 17 Allée du Six Août, 4000 Sart Tilman, Belgium
- ¹¹ *Spitzer* Science Center, California Institute of Technology, Pasadena, CA 91125, USA
- ¹² Centro Astronómico Hispano Alemán de Calar Alto (CAHA), C/ Jesús Durbán Remoñ 2-2 04004 Almería, Spain
- ¹³ NASA Exoplanet Science Institute, California Institute of Technology, Pasadena, CA 91125, USA
- ¹⁴ Jet Propulsion Lab, California Institute of Technology, 4800 Oak Grove Dr, Pasadena, CA 91109, USA
- ¹⁵ NASA Goddard Space Flight Center, Exoplanets and Stellar Astrophysics, Code 667, Greenbelt, MD 20771, USA
- ¹⁶ UNINOVA-CA3, Campus da Caparica, Quinta da Torre, Monte de Caparica, 2825-149 Caparica, Portugal
- ¹⁷ University of Kiel, Institute of Theoretical Physics and Astrophysics, Leibnizstrasse 15, 24098 Kiel, Germany
- ¹⁸ ESA Astrophysics & Fund Physics Missions Division, ESTEC/SRE-SA, Keplerlaan 1, 2201 AZ Noordwijk, The Netherlands
- ¹⁹ Astrophysikalisches Institut und Universitätssternwarte, Friedrich-Schiller-Universität, Schillergäßchen 2-3, 07745 Jena, Germany
- ²⁰ Department of Physics and Astronomy, Open University, Walton Hall, Milton Keynes MK7 6AA, UK
- ²¹ ESA/ESTEC Space Environment and Effects Section, PO Box 299, 2200 AG Noordwijk, The Netherlands
- ²² LESIA, Observatoire de Paris, 92195, Meudon, France
- ²³ Science and Technology Facilities Council, Rutherford Appleton Laboratory, Chilton, Didcot OX11 0QX, UK
- ²⁴ European Southern Observatory, Alonso de Córdova 3107, Vitacura, Santiago, Chile